



Visible Light-Activatable Platinum(IV) Prodrugs Harnessing CD36 for Ovarian Cancer Therapy

Journal:	<i>Dalton Transactions</i>
Manuscript ID	DT-ART-04-2023-001292.R2
Article Type:	Paper
Date Submitted by the Author:	04-Jul-2023
Complete List of Authors:	Jayawardhana, Amarasooriya ; Kent State University Bhandari, Srijana; Kent State University, Chemistry Kaspi-Kaneti, Ariela; Kent State University, chemistry Kshetri, Man; Kent State University Qiu, Zihan; Kent State University Cheline, May; Kent State University, Chemistry Shen, Hao; Kent State University, Chemistry and Biochemistry Dunietz, Barry; Kent State University, Chemistry Zheng, Yaorong; Kent State University,

ARTICLE

Visible Light-Activatable Platinum(IV) Prodrugs Harnessing CD36 for Ovarian Cancer Therapy

Received 00th January 20xx,
Accepted 00th January 20xx

Amarasooriya M. D. S. Jayawardhana,^a Srijana Bhandari,^a Ariela W. Kaspi-Kaneti,^{a,b} Man Kshetri,^a Zihan Qiu,^a May Cheline,^a Hao Shen,^a Barry D. Dunitz,^a and Yao-Rong Zheng^{*,a}

DOI: 10.1039/x0xx00000x

We hereby engineered photoactivatable Pt(IV) metallodrugs that harness CD36 to target ovarian cancer cells. The Pt(IV) compounds mimic the structure of fatty acids and take advantage of CD36 as a "Trojan horse" to gain entry into the cells. We confirmed that CD36-dependent entry occurs using graphite furnace atomic absorption spectroscopy with ovarian cancer cells expressing different levels of CD36 and a CD36 inhibitor, SSO. Once the Pt(IV) metallodrugs enter the cancer cells, they can be activated to form Pt(II) characteristic of cisplatin using visible light (490 nm) irradiation, which prompts photoinduced electron transfer from the attached fluorophore to the metal center. This light-induced activation can increase the cytotoxicity of the Pt(IV) metallodrugs by up to 20 times against ovarian cancer cells, inducing DNA damage and enabling efficient elimination of drug-resistant cancer cells.

Introduction

CD36 is an emerging target in cancer therapy due to its significant role in promoting tumor growth, metastasis, and drug resistance.¹⁻⁵ As a transmembrane protein that facilitates uptake of free fatty acids for lipid metabolism, CD36 provides a critical source of energy and membrane components for tumor cells.^{1, 2, 5} Recent evidence suggests that upregulation of CD36 can fuel tumor growth, metastasis, and drug resistance.¹⁻³ CD36-based therapies, such as monoclonal antibody and polypeptide treatments, have shown promise in impeding tumor metastasis.³ In ovarian tumors, CD36 is upregulated through its interaction with adipocytes in the tumor microenvironment. Studies have shown that CD36 is upregulated in both primary and metastasized ovarian tumors.^{2, 3} Despite these findings, engaging upregulation of CD36 to tackle the issue of drug resistance in ovarian cancer remains a long-standing challenge. Conventional platinum-based chemotherapy, the primary treatment for ovarian cancer, often leads to drug resistance.^{6, 7} CD36 has been found to be upregulated in drug-resistant ovarian cancer cells, however, there are still very few studies focused on addressing this issue through targeting CD36 upregulation.⁸

The approach of using photoactivatable Pt(IV) prodrugs shows promise in the development of novel Pt-based

metallodrugs that exhibit high efficacy while minimizing systemic toxicity.⁹⁻¹⁷ Compared to the cytotoxic Pt(II) payloads, the octahedral Pt(IV) complex is more resistant to ligand substitution. When reduced, the Pt(IV) complex becomes a square-planar Pt(II) center that can be released as the cytotoxic agents if the appropriate ligands are chosen.¹⁸ Photoactivation enables reduction of Pt(IV) complexes to Pt(II) products with light irradiation, which enhances the efficacy and reduces systemic toxicity in a spatiotemporally controlled manner.¹⁹⁻²¹ Studies have shown that diazido Pt(IV) complexes undergo a photo-induced reductive elimination, releasing the cytotoxic Pt(II) products upon UV light irradiation.^{19, 22-24} Additionally, flavin adenine dinucleotide has been demonstrated to act as a photocatalyst, converting Pt(IV) to cisplatin upon irradiation at 460 nm.²⁰ Moreover, recent research by Zhu has reported a series of novel carboplatin/oxaliplatin-based Pt(IV) prodrugs that can be activated by visible light.^{21, 25-27} Despite these developments, studies of visible light-activatable Pt(IV) prodrugs remain limited.

This article describes the development of the first Pt(IV) prodrug (Compound **1** in Fig. 1) that can be activated by visible light and exploits the CD36-dependent cell entry mechanism to enhance efficacy against drug-resistant ovarian cancer cells. Previous studies have demonstrated that lipophilic Pt(IV) prodrugs with hydrocarbon tails possess high potency and promising pharmacokinetics.²⁸⁻³⁶ Our recent research has also shown that such prodrugs can utilize CD36 upregulation to effectively target ovarian cancer cells.⁸ In this new project, we have modified the Pt(IV) prodrug by attaching a fluorescein moiety, which enables photoactivation upon 490-nm irradiation. By combining CD36-dependent cell entry and photoactivation, the fluorescein-Pt(IV) conjugate shows excellent efficacy in eliminating ovarian cancer cells in a

^a Department of Chemistry and Biochemistry, Kent State University, Kent, OH 44242, USA.

^b Current: Department of Chemistry, University of La Verne, 1950 3rd Street, La Verne, CA 91750, USA.

† Footnotes relating to the title and/or authors should appear here.

Electronic Supplementary Information (ESI) available: Experimental data regarding the synthesis and characterization of **1** and corresponding computational studies, cellular uptake, and flow cytometric analysis are presented in the ESI. See DOI: 10.1039/x0xx00000x

controlled manner. We also provide computational analysis of the optical properties of the complex.

Results and discussion

Synthesis and characterization of photoactivatable Pt(IV) prodrug (1). The synthesis of Pt(IV) prodrug (1) is depicted in the supporting information. Firstly, the fatty acid-like Pt(IV) prodrug (C16Pt) was synthesized using a reported procedure.⁸ Next, it was conjugated with fluorescein thiocarbamylethylenediamine via the HATU-catalyzed amide bond formation reaction. The overall yield was 80.7%. The fluorescein-conjugated Pt(IV) compound (1) was characterized using ¹H and ¹³C NMR spectroscopy, electrospray ionization mass spectrometry (ESI-MS), and HPLC. The broad signal at 6.5 ppm in the ¹H NMR spectrum (Fig S1B in Supporting Information) corresponds to the amine groups of the Pt(IV) center and fluorescein, while the signals at 0.85 ppm and 1.20 ppm are from the C16 tail attached to the carbamate. The isotopically resolved signal at *m/z* = 1133.3343 in the ESI-MS spectrum (Fig S1D) agrees with the theoretical value of 1 (*m/z* = 1133.3340). HPLC analysis of the final product indicated a purity of 96% using the described synthetic method.

CD36-dependent cell entry of the Pt(IV) prodrug (1). We conducted further experiments to investigate the ability of the Pt(IV) prodrug (1) to harness CD36 for facilitating its cell entry in drug-resistant ovarian cancer cells. Specifically, we evaluated the CD36-dependent cell entry of compound 1 by using both a cisplatin-sensitive ovarian cancer cell line (A2780) and its cisplatin-resistant counterpart (A2780cis). We performed Western blot analysis to assess the expression of CD36 in both cell lines. As shown in Fig 2A, CD36 was found to be expressed in A2780cis cells, but not in A2780 cells, which is consistent with our previous findings.⁸ Based on this, we hypothesized that the upregulation of CD36 could facilitate the cell

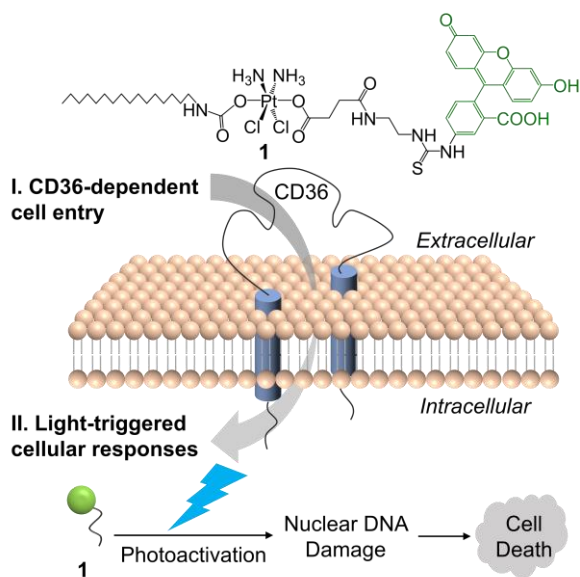


Fig 1. Graphical representation of mechanism of action of the visible light-activatable Pt(IV) prodrug (1).

entry of 1. We then used graphite furnace atomic absorption spectroscopy (GFAAS) to measure the cellular uptake of 1 in both cell lines. The results showed that 1 preferentially accumulated in A2780cis cells (179±5 pmol Pt/μg proteins) compared to A2780 cells (77.4±1.4 pmol Pt/μg proteins), but cisplatin did not exhibit any significant difference in intracellular accumulation across these cell lines. Furthermore, we used Sulfo-N-succinimidyl oleate (SSO) to inhibit CD36-dependent cell entry of compound 1. SSO is a fatty acid-like small molecule that blocks CD36-dependent cell entry by covalently binding to the protein. As shown in Fig S2 in the supporting information, the preferential uptake of 1 in A2780cis cells was considerably hampered by pre-treatment with SSO. However, despite the inhibition by SSO, the high lipophilicity of 1 allowed for its superior uptake compared to that of cisplatin.

Photoactivation of the Pt(IV) prodrug (1). In the next step, we evaluated the photoactivation of the Pt(IV) prodrug (1) and its light-triggered cellular responses *in vitro*. We hypothesized that the photoactivation of 1 leads to the release of a fluorescein derivative (2) and cisplatin, as shown in Fig 3A. To validate our hypothesis, we employed fluorescence spectroscopy, cellular imaging, and flow cytometry. Upon a 20-minute exposure to 490-nm light (2.36 mW/cm²), we observed fluorescence turn-on in 1 due to the cleavage of the fluorescein derivative from the heavy metal center, as depicted in Fig 3B. In addition, we verified the fluorescence turn-on phenomenon in live cells that were treated with the Pt(IV) prodrug 1 and exposed to 490-nm irradiation, as demonstrated in Fig 3C. Next, we utilized flow cytometry to investigate the extent of nuclear DNA damage by analyzing the extent of phosphorylation of H2AX (γH2AX), a known biomarker of DNA damage, since cisplatin is known to target nuclear DNA. Our results demonstrated that treatment of the Pt(IV) prodrug (1) with 490-nm irradiation resulted in a significant increase in γH2AX, indicating light-triggered nuclear DNA damage, as evidenced in Fig 3D. In contrast, treatment of 1 alone in the dark did not cause significant nuclear damage, suggesting that most of the Pt payloads were not activated without light. We further employed cellular imaging studies and flow cytometric analysis to confirm that light-triggered nuclear DNA damage ultimately resulted in cell death. As demonstrated by the live-death cell assays results in Fig 3E, the

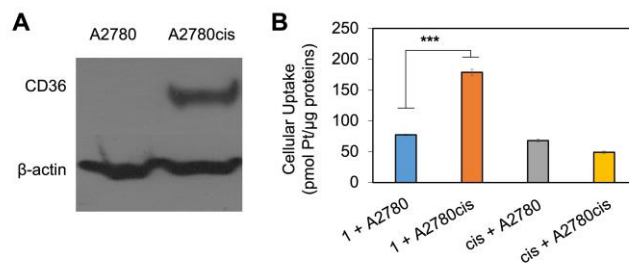


Fig 2. CD36-dependent cellular entry and cytotoxicity profiles of the visible light-activatable Pt(IV) prodrug (1): **A.** Western blot analysis of CD36 expression in A2780 and A2780cis ovarian cancer cells; **B.** GFAAS measurement of cellular uptake of 1 and cisplatin (cis) against A2780 (left) and A2780cis (right) cells (10 μM, 4 h). ****P*<0.0005. by *t* test (*n*=3, mean ± SEM).

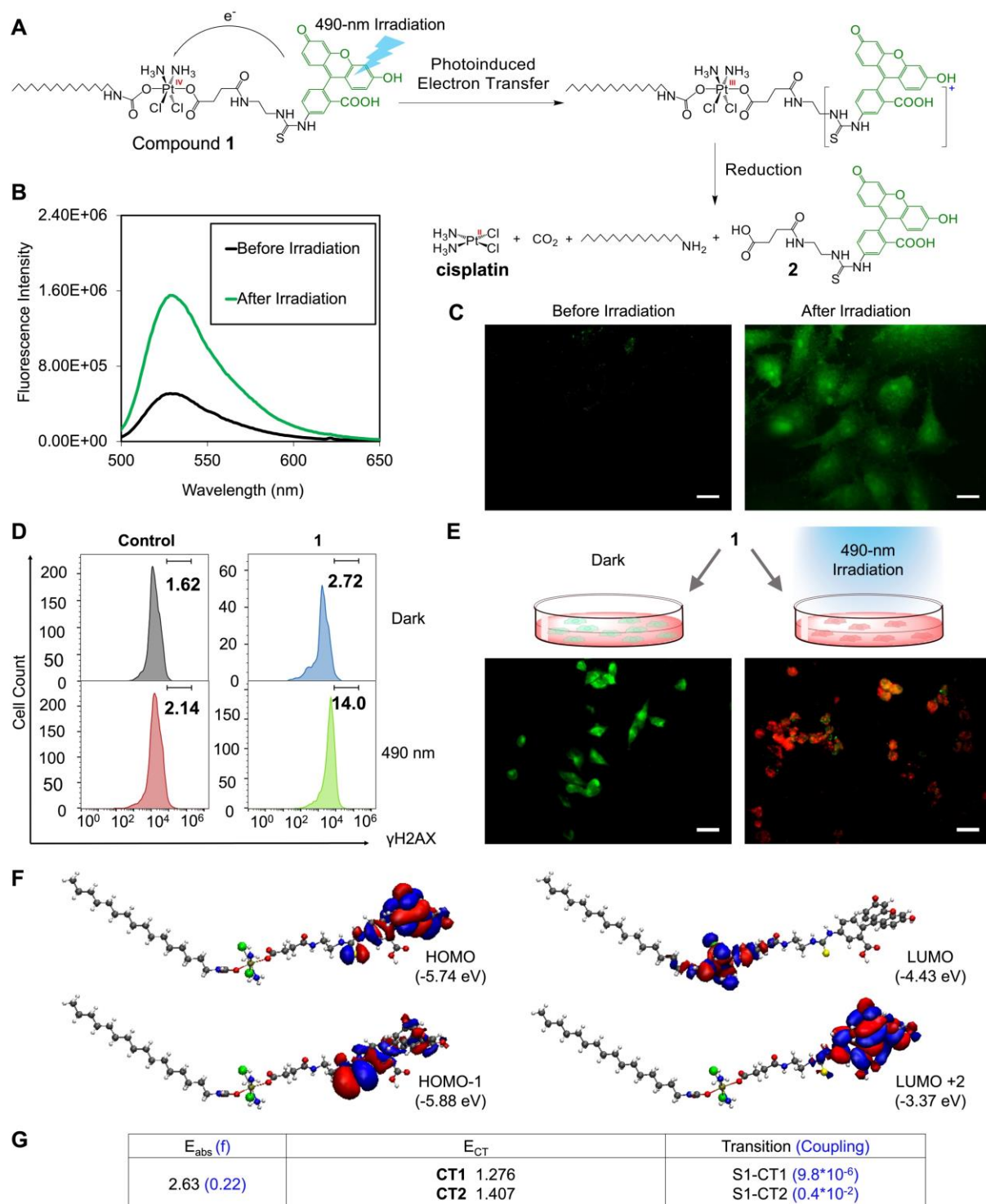


Fig 3. Photoinduced electron transfer empowers the photoactivation of the Pt(IV) prodrug (**1**): **A.** Graphical representation of the photoactivation process: 490-nm irradiation facilitates photoinduced electron transfer from the fluorescein dye to the Pt(IV) center, leading to the formation of the Pt(III) intermediate. This intermediate is rapidly reduced to release the axial ligands and the Pt(II) species, triggering subsequent cellular responses, including nuclear DNA damage and cell death; **B.** Fluorescence spectra of Compound **1** in PBS recorded before and after 20-min irradiation of 490-nm light (2.36 mW/cm²); **C.** Fluorescence images of the **1**-treated A549 cells (10 μM, 6 h) recorded before and after 20-min irradiation of 490-nm light; **D.** Flow cytometric analysis of nuclear DNA damage of the A2780cis cells without (*left*, Control) and with the treatment of **1** (*right*, 10 μM, 6 h) in the absence (Dark) or presence (490 nm) of 20-min irradiation by 490 nm light (2.36 mW/cm²); **E.** Fluorescence images of the live (green)/dead (red) assays of the A2780cis cells treated with **1** ([Pt] = 20 μM, 6 h) recorded without (*left*) or with (*right*) 490-nm irradiation. Scale bar is 20 μm; **F.** Electronic distributions of the HOMO-1, HOMO, LUMO, and LUMO+2 of **1**; **G.** Electronic excited state energies and the oscillator strength of the absorbing state (S1), electronic coupling of S1 with the CT states.

treatment of **1** (20 μM , 6 h) and 490-nm irradiation induced cell death in A2780cis cells. In contrast, the cells treated with **1** in the dark did not show cell death. Flow cytometric analysis (Fig S3) further confirmed that a large population of the **1**-treated cells underwent cell death in response to light irradiation. Therefore, the photoactivation of the Pt(IV) prodrug is found to release cisplatin payloads, which induces light-triggered nuclear damage and subsequent cell death.

Computational analysis of the photoactivation process. We investigated the photoactivation of prodrug (**1**). In Fig 3A we illustrate the proposed mechanism, where photoexcitation of fluorescein dye by 490-nm visible light induces electron transfer to the Pt(IV) center, forming a Pt(III) intermediate. This intermediate is rapidly reduced to the Pt(II) species. Our calculations resolve the relevant excited states of **1** to the photoinduced electron transfer step.^{24, 25} In the Pt complex, the calculated excitation energy of the absorbing state is 2.63 eV (oscillator strength [OS] of 0.22, involving mostly the replacement of the highest occupied molecular orbital (HOMO) by the lowest unoccupied molecular orbital (LUMO+2), that is red shifted compared to 2.89 eV (OS of 0.51) for the free fluorescein and is in good agreement with the measured value of 2.53 eV (equivalent to 490 nm). The two lowest CT states, CT1 of 1.28 eV and CT2 of 1.41 eV, involve electron transfer from the fluorescein (donor) towards the Pt(IV) center (acceptor). The CT1 and CT2 states are dominated by the replacement of the HOMO and HOMO-1, respectively, by LUMO (See Fig 3F for illustrating the orbitals). Both HOMO and HOMO-1 are localized in the fluorescein moiety, where the LUMO is localized towards the Pt(IV) center. Fig 3G lists the excitation energies of the S1 and CT states and the S1 to CT coupling energies. The CT process involving the CT2 state is indicated to dominate the reduction process leading to Pt(III). The coupling between the absorbing state to CT2 is 4.0×10^{-3} eV, while that to CT1 is significantly smaller, effectively vanishing with 9.8×10^{-6} eV. Overall, these results support the assertion that electron transfer follows the photoexcitation to affect the reduction of the Pt(IV) prodrug.

Cytotoxicity profiles of the Pt(IV) prodrug (1**).** Our primary objective was to evaluate the cytotoxicity of **1** and establish its association with CD36 expression and light exposure. To determine the viability of cells with varying levels of CD36 that were treated with **1** and light irradiation, we employed 3-(4,5-dimethylthiazol-2-yl)-2,5-diphenyltetrazolium bromide (MTT) assays. The IC_{50} values, which indicate the concentration required to inhibit growth by 50%, are illustrated in Fig 4A. In the absence of 490-nm irradiation (Dark), **1** exhibits a similar cytotoxicity profile as cisplatin. Notably, upon irradiation, the IC_{50} values of **1** were decreased to 8.40 ± 0.50 μM in A2780 and 8.55 ± 0.80 μM in A2780cis, which is up to 20 times more potent compared to cisplatin. In the absence of light, most of the payloads are not in the active form. So, even though cellular uptake of **1** excels that of cisplatin, **1** is still of low potency. In the dark, **1** demonstrates significantly lower cytotoxicity compared to C16Pt. Once light irradiation is applied, the payloads are activated, resulting in much higher potency, and that surpasses that of C16Pt.

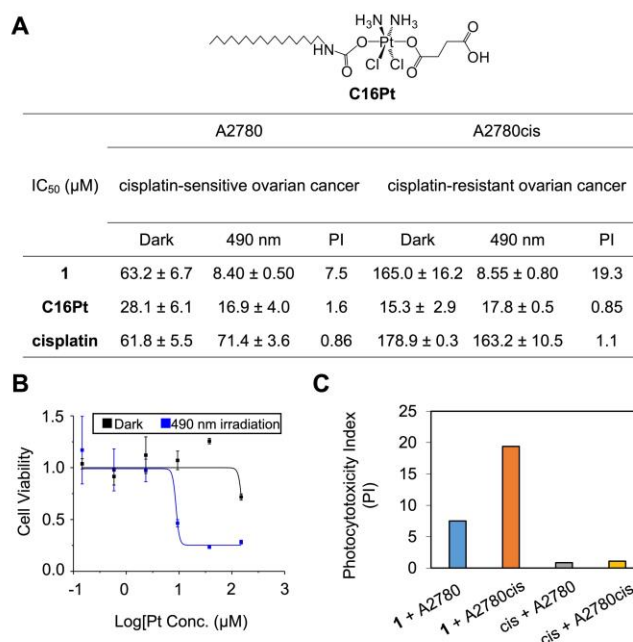


Fig 4. Cytotoxicity profiles of the visible light-activatable Pt(IV) prodrug (**1**): **A**. The table of IC_{50} values and phototoxicity index (PI) determined by MTT assays for **1**, C16Pt, and cisplatin against A2780 and A2780cis with 24-h incubation in the absence (Dark) or presence (490 nm) of 20-min irradiation by 490 nm light (2.36 mW/cm^2); **B**. Representative killing curves of **1** against A2780cis cells; **C**. Bar graph of the phototoxicity indexes (PI) of **1** and cisplatin against A2780 and A2780cis cells.

Accordingly, we calculated the phototoxicity indexes (PI) of **1** based on $\text{IC}_{50}(\text{Light})/\text{IC}_{50}(\text{Dark})$ as shown in Fig 4A. Interestingly, **1** exhibits a much higher PI (19.3) against A2780cis compared to A2780 (7.5). This is consistent with the CD36-dependent uptake described above. The upregulated CD36 in A2780cis facilitates twice of payload accumulation as that in A2780. In sum, these results support that the photoactivatable Pt(IV) prodrug (**1**) harnesses CD36 to facilitate their cell entry toward killing A2780cis cisplatin-resistant CD36-overexpressing ovarian cancer cells in a light-controlled manner.

Conclusions

In conclusion, we have presented a novel chemical design for Pt(IV) prodrugs that are activated by visible light and exploit the upregulated CD36 to enhance cellular uptake in ovarian cancer. In this design, the fluorescein axial ligand captures 490-nm photon flux and induces photoinduced electron transfer for the reduction (or activation) of the Pt(IV) prodrugs, leading to light-induced cellular responses such as nuclear DNA damage and cell death. Notably, the other lipophilic axial ligand of the Pt(IV) centers promotes CD36-dependent cell entry, making it effective against CD36-upregulated cisplatin-resistant ovarian cancer cells. This work represents a proof-of-concept study towards developing tumor-specific photoactivatable metallodrugs. The photoactivation mechanism may mitigate off-target effects resulting from CD36 expression in normal

tissues, making it a promising approach for future translational applications.

Experimental

General information. All reagents were purchased from Strem, Sigma Aldrich or Alfa Aesar and used without further purification. Fluorescein thiocarbamylethylenediamine was synthesized according to the reported literature.³⁷ All reactions were carried out under normal atmospheric conditions. A Bruker 400 NMR was used for NMR data acquisition (Frequency: 400 MHz for ¹H NMR; 100 MHz for ¹³C NMR) and the plots were generated by TOPSPIN 3.2 software. Chemical shifts in ¹H and ¹³C NMR spectra were internally referenced to solvent signals (¹H NMR: DMSO at $\delta = 2.50$ ppm; ¹³C NMR: DMSO at $\delta = 39.51$ ppm). The high-resolution mass spectra of created ions were recorded on an Exactive Plus mass spectrometer (Thermo Scientific, Bremen, Germany). Blue LED light source is Kessil A160WE. The photon flux at 490 nm was determined using a Thorlabs optical power meter, and it is 2.36 mW/cm². GFAAS measurements were taken on a PerkinElmer PinAAcle 900Z spectrometer. The Pt concentrations for all the studies have been quantified using GFAAS. Elemental analysis was performed on a TruSpec Micro, CHNS analyzer from LECO Corporation. Fluorescence spectra were taken on FluoroMax-3 Fluorescence spectrophotometer using the software called FluorEssence. Fluorescence images were acquired using an Olympus IX70 inverted epifluorescence microscope equipped with a digital CCD camera (QImaging). Images were processed and intensities were quantified with ImageJ software (NIH). Flow cytometry was carried out on a FACSAria™II flow cytometer. Live/Dead cell assay was carried out using Invitrogen (Thermo Fisher Scientific) LIVE/DEAD™ Cell Viability Kit (Cat. No. L3224).

Synthesis of Compound 1. To the mixture of C16Pt (39.2 mg, 0.056 mmol) and HATU (21.3 mg, 0.056 mmol) was added 1 mL anhydrous DMF. The solution was stirred for 20 min at r.t. Then, to the reaction mixture, 0.4 mL anhydrous DMF solution of fluorescein thiocarbamylethylenediamine (30 mg, 0.067 mmol) was added. After 30 min of stirring at r.t., DIPEA (19 μ L, 0.112 mmol) was added. The vial was covered by aluminum foil, and the reaction mixture was stirred for 6 h at r.t.. A total of 4 mL brine was added to the reaction mixture to precipitate the product. Then, the precipitation was collected by centrifuge, and washed with excess of water. The final product was obtained after lyophilization. Yield: 52.0 mg (80.7%). ¹H NMR (400 M Hz, DMSO-d₆) : δ : 0.852 (NHCH₂(CH₂)₁₄CH₃, t, J= 6.8 Hz, 3H), 1.232 (NHCH₂(CH₂)₁₄CH₃, m, 28H), 2.247-2.477 (COCH₂CH₂CO, m, 4H), 2.740-2.838 (NHCH₂CH₂NH-FITC, m, 4H), 3.207-3.275 (NHCH₂(CH₂)₁₄CH₃, m, 2H), 6.505-6.672 (NH₃, NHCH₂(CH₂)₁₄CH₃, FITC, m, 13H), 7.176 (FITC, d, J=8.4Hz, 1H), 7.809 (FITC, s, 1H), 7.964 (NHCH₂CH₂NH-FITC, t, J=5.6 Hz, 2H), 8.223 (FITC, s, 2H); ¹³C NMR (100 MHz, DMSO-d₆) : δ : 180.3, 174.3, 172.8, 172.0, 169.0, 164.4, 160.0, 152.3, 129.5, 113.0, 110.2, 102.7, 41.5, 38.8, 37.5, 31.9, 31.7, 30.5, 30.4, 29.5, 29.4, 29.3, 29.2, 26.9, 26.2, 22.5, 14.4. Anal. Calcd for

C₄₄H₆₂Cl₂N₆O₁₀PtS·(H₂O)₃: C, 44.52; H, 5.77; N, 7.08. Found: C, 44.29; H, 5.52; N, 7.17. HR-MS (positive mode) for [C₄₄H₆₂Cl₂N₆O₁₀PtS+H]⁺: m/z calc: 1133.3340, m/z obsd: 1133.3343; Purity: 96% determined by HPLC.

Western Blotting experiments for CD36 expression in A2780 and A2780cis cell line. A2780 and A2780cis cells were collected and lysed by RIPA buffer. 2X loading dye was added into the protein samples. The samples were heated at 100 °C for 7-10 min, and quick centrifuged. Meantime, the gel electrophoresis equipment was setup, and the 1X running buffer was filled in the tank. The denatured protein samples were injected into the SDS-PAGE gel, 20 μ g/well. The gel was run at 200V, 38min and transferred to a sandwich structure model to be prepared for gel transfer, which used PVDF membrane to catch the proteins. The gel transfer took 90 min at 28V by wet transfer. The PVDF membrane was cut off based on the MW of the proteins (CD36 85-90 KDa, β -actin 45 KDa). The membrane was put in block buffer and gently shaken at r.t. for 1h. The membrane was incubated by the primary antibodies of CD36 (BioLegend®, San Diego, CA, USA) and β -actin overnight at 4 °C with gently shaking. The membrane was washed by 1X TBST 3 times at R.T., and 10min for each with gently shaking. The membrane was incubated with secondary antibody at r.t. for 1h with gently shaking. The membrane was washed by 1X TBST 3 times again at r.t., and 10min for each with gently shaking. The ECL substrate was applied on the membrane. A western blotting (WB) film was covered on the membrane and pressed for few second in a dark room, and an X-ray film processor was used to detect and analyse chemiluminescence signal of WB.

GFAAS analysis of cellular Pt contents of A2780 and A2780cis cells. A2780 and A2780cis cells were seeded in a 6-well plate at a concentration of 2×10^5 cells per well and incubated at 37 °C, 5% CO₂ overnight. These cells were treated with cisplatin or Compound **1** ([Pt] = 10 μ M) for 4 h at 37 °C, 5% CO₂. The remaining alive cells were harvested by trypsinization and counted. The cells were then digested in 200 μ L 65% HNO₃ at r.t. overnight. The Pt contents in the cells were analyzed by GFAAS. All experiments were performed in triplicate.

GFAAS analysis of cellular Pt contents of A2780cis cells treated with SSO. A2780cis cells were seeded in a 6-well plate at a concentration of 2×10^5 cells per well and incubated at 37 °C, 5% CO₂ overnight. The cells were treated with 200 μ M sulfo-N-succinimidyl oleate (SSO, Cayman Chemical Company, Michigan, USA) in RPMI media without FBS and PS to avoid the fatty acid presence in FBS, and incubated 30 min at 37 °C, 5% CO₂. Then, the RPMI media was removed and fresh complete RPMI media was added in the wells. Compound **1** or cisplatin (10 μ M) was added into cells and incubated 4 h at 37 °C, 5% CO₂. The Pt contents in the cells were analyzed by GFAAS following the abovementioned procedure.

Fluorescence spectra of Compound 1 with and without 20-min irradiation by 490 nm light. 80 μ M solution of Compound **1** was prepared in PBS (Phosphate Buffer Saline) at r.t.. Fluorescence

emission spectra was taken on FluoroMax-3 fluorescence spectrophotometer for 500–650 nm range with excitation at 490 nm. Next, the solution was irradiated with 490 nm LED for 20-min and spectra was taken again.

Florescence imaging experiments for A549 cells treated with Compound 1 with and without 20-min irradiation by 490 nm light. A549 cells were seeded in two imaging disks (MatTek) at a concentration of 5×10^4 cells with 2 mL of complete medium and incubated for 24 h at 37 °C. The cells in both disks were then treated with Compound 1 (10 μ M) and incubated for 6 h at 37 °C, 5% CO₂. Next, one disk was irradiated with 490 nm LED for 20 minutes. Both disks were washed 3 times with 1 mL of PBS and images were acquired using an Olympus IX70 inverted epifluorescence microscope equipped with a digital CCD camera (QImaging). Images were processed and intensities were quantified with ImageJ software (NIH).

Flow cytometric analysis of nuclear damage using γ H2AX. A2780cis cells seeded in 3 wells of two 6-well plates at a concentration of 2×10^5 cells/well and incubated for 24 h at 37 °C, 5% CO₂. Next, the cells were treated with cisplatin or Compound 1 (10 μ M) while the third well was kept as a control. Cells were then incubated for 6 h at 37 °C, 5% CO₂. After 6 h, one well plate was irradiated with 490 nm LED for 20 minutes. Both well plates were washed with fresh medium and filled with 5mL fresh medium. Plates were then incubated for 24 h at 37°C, 5% CO₂. Next, the live cells were collected and washed with 1mL PBS. 250 μ L BD Permeabilization solution was added to re-suspend the cells and incubated for 20 min at 4 °C. The cell pellet was collected and washed twice with 1 mL 1 x wash buffer. To the pellet with 50 μ L of buffer, 5 μ L Alexa Fluor 647-anti H2AX antibody solution was added and incubated in the dark for 60 min at r.t.. Centrifuged (1400 rpm, 5 min) and the cell pellet was suspended in 300 μ L of PBS and analyzed using a flow cytometry APC channel on a FACSAria™II flow cytometer (BD Biosciences, Franklin Lakes, NJ, USA).

Flow cytometric analysis cell death using propidium iodide (PI). A2780cis cells seeded in 3 wells of two 6-well plates at a concentration of 2×10^5 cells/well and incubated for 24 h at 37 °C. Next, the cells were treated with cisplatin or Compound 1 (20 μ M) while the third well was kept as a control. Cells were then incubated for 6 h at 37 °C. After 6 h, one well plate was irradiated with 490 nm LED for 20 minutes. Both well plates were washed with fresh medium and filled with 5mL fresh medium. Plates were then incubated for 24 h at 37 °C. Next, the medium was collected in clean 15 mL falcon tubes along with washed PBS solution. 1mL trypsin was added to the wells. After 5 min, cell suspensions were transferred to the falcon tubes that contained the media and PBS and centrifuged at 400–500x g at 4 °C for 5min. The cell pellet was re-suspended in 1 mL PBS and the cells were counted. The cell pellet was collected again and the appropriate amount of 1x binding buffer was added to reach a concentration of 10^6 cells/mL. 100- μ L cell suspensions were added to new 2-mL Eppendorf tubes and 5 μ L of PI solution was added. Cells were gently vortexed and incubated at r.t. for 15

min in the dark. 400- μ L 1x binding buffer was added to each Eppendorf tube and the cell suspensions were transferred to flow cytometry tubes. Flow cytometry analysis was done using PerCP/Cy5.5 channel on a FACSAria™II flow cytometer (BD Biosciences, Franklin Lakes, NJ, USA).

LIVE/DEAD cell viability assays. A2780cis cells were cultured in two imaging disks (MatTek) at a concentration of 5×10^4 cells with 2 mL of complete medium and incubated for 24 h at 37 °C. The cells in both disks were then treated with Compound 1 (20 μ M) and incubated for 6 h at 37 °C, 5% CO₂. Next, one disk was irradiated with 490 nm LED for 20 minutes. Medium in both disks were replaced with new RPMI complete medium and incubated overnight. Before the assay, the cells were washed with 1 mL PBS and 1 mL dye-free RPMI to remove serum esterase activity generally present in serum-supplemented growth media. A 500 μ L volume of LIVE/DEAD working solution (formed by mixing 2 μ M of calcein AM and 2 μ M ethidium homodimer-1 in PBS) was carefully added to the disks, which were then incubated at r.t. for 30 min. Images were acquired using an Olympus IX70 inverted epifluorescence microscope equipped with a digital CCD camera (QImaging). Images were processed and intensities were quantified with ImageJ software (NIH).

Computational methods. Fluorescein and Compound 1 are optimized in their ground state using density functional theory (DFT) at the B3LYP/6-31G* level for O, N, C, H, Cl and S atoms and LANL2DZ effective core potential for the Pt atom, in PCM representing water as the solvent. All the excited state calculations were performed using time dependent DFT (TDDFT) with screened range separated hybrid (SRSH) based on PBE functional with PCM.^{38, 39} The SRSH-PCM is a recently developed framework that is based on a polarization consistent framework between the functional parameters determining the weight of the exact exchange at long range and the reaction field implementing the PCM, where the same dielectric constant is invoked. The optimally tuned parameter for the fluorescein was tuned following the J2 scheme and was found 0.148 bohr⁻¹ in the gas phase, and where the beta parameter is reset according to the dielectric constant³⁸. The same tuned value was used for the complex. All calculations were performed using Q-Chem v5.⁴⁰ Electronic state coupling energies are calculated used fragment charge differences [jcp, 177, 5607]

MTT assays of cisplatin, C16Pt, and 1 against A2780 and A2780cis cells with and without 20-min irradiation by 490 nm light. The cells (A2780 and A2780cis) were seeded in 96-well microplates (two plates from each cell line) in 100 μ L cell suspensions (2×10^4 cells per mL) per well to begin and were incubated for 24 h at 37 °C, 5% CO₂. Next, 50 μ L volume of RPMI with various concentrations of Pt compounds was added to each well of the microplates. The cells were then incubated for an additional 6 h at 37 °C, 5% CO₂. Next, one plate was kept in the dark and other plate was irradiated with 490 nm LED for 20 minutes. After the irradiation, medium in both plates were

aspirated out and filled with 150 μL of fresh medium followed by one time washing with 200 μL fresh medium. The plates were then incubated for 24 h at 37 $^{\circ}\text{C}$, 5% CO_2 . Next, a volume of 30 μL MTT (Alfa Aesar) (5 mg mL^{-1} in PBS) was added to the cells and then the cells were incubated for an additional 2-4 h at 37 $^{\circ}\text{C}$, 5% CO_2 . The solutions were then aspirated, leaving behind insoluble purple formazan. A volume of 200 μL DMSO was added to the wells and the plates were shaken for 10 min. Next, the microplates were analyzed for absorbance at 562 nm with an ELx800 absorbance reader (BioTek, Winooski, VT, USA). Finally, the data were analyzed using Origin software to produce dose-response curves and to determine IC_{50} values. All experiments were performed in triplicate.

Conflicts of interest

There are no conflicts to declare.

Acknowledgements

Y.-R. Z thanks the financial support provided by the R15 grant (1R15CA249712-01A1) provided by National Cancer Institute and the Farris Family Innovation Fellowship and LaunchPad Award provided by Kent State University. Y.-R. Z thanks the support from The Research Council of Kent State University. B.D.D. acknowledges support by the Department of Energy, basic energy sciences grant no. DE-SC0016501 and Kent State University for partial support and for generous resource allocation on the Ohio Supercomputer Center (project PAA-0213). A. M. D. S. J. thanks the financial support provided by Healthy Communities Research Initiative at Kent State University.

Notes and references

- G. Pascual, A. Avgustinova, S. Mejetta, M. Martin, A. Castellanos, C. Attolini, A. Berenguer, N. Prats, A. Toll, J. Huetto, C. Bescos, L. Di Croce and S. Benitah, *Nature*, 2017, **541**, 41.
- A. Ladanyi, A. Mukherjee, H. Kenny, A. Johnson, A. Mitra, S. Sundaresan, K. Nieman, G. Pascual, S. Benitah, A. Montag, S. Yamada, N. Abumrad and E. Lengyel, *Oncogene*, 2018, **37**, 2285-2301.
- S. Wang, A. Blois, T. El Rayes, J. Liu, M. Hirsch, K. Gravdal, S. Palakurthi, D. Bielenberg, L. Akslen, R. Drapkin, V. Mittal and R. Watnick, *Sci Trans Med*, 2016, **8**.
- W. W. Feng, O. Wilkins, S. Bang, M. Ung, J. Li, J. An, C. Del Genio, K. Canfield, J. DiRenzo, W. Wells, A. Gaur, R. B. Robey, J. Y. Guo, R. L. Powles, C. Sotiriou, L. Pusztai, M. Febbraio, C. Cheng, W. B. Kinlaw and M. Kurokawa, *Cell Rep*, 2019, **29**, 3405-3420.e3405.
- M. J. Watt, A. K. Clark, L. A. Selth, V. R. Haynes, N. Lister, R. Rebello, L. H. Porter, B. Niranjana, S. T. Whitby, J. Lo, C. Huang, R. B. Schittenhelm, K. E. Anderson, L. Furic, P. R. Wijayarathne, M. Matzaris, M. K. Montgomery, M. Papargiris, S. Norden, M. Febbraio, G. P. Risbridger, M. Frydenberg, D. K. Nomura and R. A. Taylor, *Sci Transl Med*, 2019, **11**.
- D. Wang and S. J. Lippard, *Nat. Rev. Drug Discovery*, 2005, **4**, 307-320.
- D. Holmes, *Nature*, 2015, **527**, S218-219.
- A. M. D. S. Jayawardhana, M. Stilgenbauer, P. Datta, Z. Qiu, S. McKenzie, H. Wang, D. Bowers, M. Kurokawa and Y. R. Zheng, *Chem Commun*, 2020, **56**, 10706-10709.
- M. D. Hall and T. W. Hambley, *Coord. Chem. Rev.*, 2002, **232**, 49-67.
- E. Wexselblatt and D. Gibson, *J. Inorg. Biochem.*, 2012, **117**, 220-229.
- Z. Dai and Z. Wang, *Molecules*, 2020, **25**.
- H. Lu, S. He, Q. Zhang, X. Li, Z. Xie, Z. Wang, Y. Qi and Y. Huang, *Biomater Sci*, 2021, **9**, 7115-7123.
- M. Imran, W. Ayub, I. S. Butler and R. Zia ur, *Coord Chem Rev*, 2018, **376**, 405-429.
- K. Mitra, C. E. Lyons and M. C. T. Hartman, *Angew Chem Int Ed Engl*, 2018, **57**, 10263-10267.
- J. A. Roque lli, H. D. Cole, P. C. Barrett, L. M. Lifshits, R. O. Hodges, S. Kim, G. Deep, A. Francés-Monerris, M. E. Alberto, C. G. Cameron and S. A. McFarland, *J Am Chem Soc*, 2022, **144**, 8317-8336.
- A. Mani, T. Feng, A. Gandioso, R. Vinck, A. Notaro, L. Gourdon, P. Burckel, B. Saubaméa, O. Blacque, K. Cariou, J.-E. Belgaied, H. Chao and G. Gasser, *Angew Chem Int Ed Engl*, 2023, **n/a**, e202218347.
- D. Havrylyuk, A. C. Hachey, A. Fenton, D. K. Heidary and E. C. Glazer, *Nature Commun*, 2022, **13**, 3636.
- A. W. Kaspi-Kaneti, S. Bhandari, A. Schubert, S. D. Huang and B. D. Dunietz, *Chemphyschem*, 2021, **22**, 106-111.
- F. S. Mackay, J. A. Woods, P. Heringová, J. Kaspárková, A. M. Pizarro, S. A. Moggach, S. Parsons, V. Brabec and P. J. Sadler, *Proc Natl Acad Sci U S A*, 2007, **104**, 20743-20748.
- M. Martinez-Calvo and J. Mascarenas, *Coord Chem Rev*, 2018, **359**, 57-79.
- Z. Wang, N. Wang, S.-C. Cheng, K. Xu, Z. Deng, S. Chen, Z. Xu, K. Xie, M.-K. Tse, P. Shi, H. Hirao, C.-C. Ko and G. Zhu, *Chem*, 2019, **5**, 3151-3165.
- C. Imberti, P. Zhang, H. Huang and P. J. Sadler, *Angew Chem Int Ed Engl*, 2020, **59**, 61-73.
- H. Shi, I. Romero-Canelón, M. Hreusova, O. Novakova, V. Venkatesh, A. Habtemariam, G. J. Clarkson, J. I. Song, V. Brabec and P. J. Sadler, *Inorg Chem*, 2018, **57**, 14409-14420.
- N. J. Farrer, L. Salassa and P. J. Sadler, *Dalton Trans*, 2009, 10690-10701.
- Z. Deng, N. Wang, Y. Liu, Z. Xu, Z. Wang, T. C. Lau and G. Zhu, *J Am Chem Soc*, 2020, **142**, 7803-7812.
- H. Yao, S. Chen, Z. Deng, M. K. Tse, Y. Matsuda and G. Zhu, *Inorg Chem*, 2020, **59**, 11823-11833.
- Z. Deng, C. Li, S. Chen, Q. Zhou, Z. Xu, Z. Wang, H. Yao, H. Hirao and G. Zhu, *Chem Sci*, 2021, **12**, 6536-6542.
- Y.-R. Zheng, K. Suntharalingam, T. C. Johnstone, H. Yoo, W. Lin, J. G. Brooks and S. J. Lippard, *J. Am. Chem. Soc.*, 2014, **136**, 8790-8798.
- M. Miller, Y. Zheng, G. Suresh, C. Pfirschke, H. Zope, C. Engblom, R. Kohler, Y. Iwamoto, K. Yang, B. Askevold,

- N. Kolishetti, M. Pittet, S. Lippard, O. Farokhzad and R. Weissleder, *Nature Commun*, 2015, **6**.
30. M. Stilgenbauer, A. M. D. S. Jayawardhana, P. Datta, Z. Yue, M. Gray, F. Nielsen, D. J. Bowers, H. Xiao and Y. R. Zheng, *Chem Commun*, 2019, **55**, 6106-6109.
31. A. M. D. S. Jayawardhana and Y. R. Zheng, *Dalton Trans*, 2022, **51**, 2012-2018.
32. D. Wei, Y. Yu, X. Zhang, Y. Wang, H. Chen, Y. Zhao, F. Wang, G. Rong, W. Wang, X. Kang, J. Cai, Z. Wang, J. Y. Yin, M. Hanif, Y. Sun, G. Zha, L. Li, G. Nie and H. Xiao, *ACS Nano*, 2020, **14**, 16984-16996.
33. F. Zhou, B. Feng, H. Yu, D. Wang, T. Wang, Y. Ma, S. Wang and Y. Li, *Adv Mater*, 2019, **31**, e1805888.
34. X. Kang, Y. Wang, Z. Chen, Y. Wu, H. Chen, X. Yang and C. Yu, *Chem Commun*, 2020, **56**, 11271-11274.
35. J. Ma, Q. Wang, Z. Huang, X. Yang, Q. Nie, W. Hao, P. G. Wang and X. Wang, *J Med Chem*, 2017, **60**, 5736-5748.
36. A. Abu Ammar, R. Raveendran, D. Gibson, T. Nassar and S. Benita, *J Med Chem*, 2016, **59**, 9035-9046.
37. R. Gentsch, F. Pippig, K. Nilles, P. Theato, R. Kikkeri, M. Magliano, B. Lepenies, P. H. Seeberger and H. G. Börner, *Macromolecules*, 2010, **43**, 9239-9247.
38. S. Bhandari, M. S. Cheung, E. Geva, L. Kronik and B. D. Dunietz, *J Chem Theory Comput*, 2018, **14**, 6287-6294.
39. S. Bhandari and B. D. Dunietz, *J Chem Theory Comput*, 2019, **15**, 4305-4311.
40. E. Epifanovsky, A. T. B. Gilbert, X. Feng, J. Lee, Y. Mao, N. Mardirossian, P. Pokhilko, A. F. White, M. P. Coons, A. L. Dempwolff, Z. Gan, D. Hait, P. R. Horn, L. D. Jacobson, I. Kaliman, J. Kussmann, A. W. Lange, K. U. Lao, D. S. Levine, J. Liu, S. C. McKenzie, A. F. Morrison, K. D. Nanda, F. Plasser, D. R. Rehn, M. L. Vidal, Z. Q. You, Y. Zhu, B. Alam, B. J. Albrecht, A. Aldossary, E. Alguire, J. H. Andersen, V. Athavale, D. Barton, K. Begam, A. Behn, N. Bellonzi, Y. A. Bernard, E. J. Berquist, H. G. A. Burton, A. Carreras, K. Carter-Fenk, R. Chakraborty, A. D. Chien, K. D. Closser, V. Cofer-Shabica, S. Dasgupta, M. de Wergifosse, J. Deng, M. Diedenhofen, H. Do, S. Ehlert, P. T. Fang, S. Fatehi, Q. Feng, T. Friedhoff, J. Gayvert, Q. Ge, G. Gidofalvi, M. Goldey, J. Gomes, C. E. González-Espinoza, S. Gulania, A. O. Gunina, M. W. D. Hanson-Heine, P. H. P. Harbach, A. Hauser, M. F. Herbst, M. Hernández Vera, M. Hodecker, Z. C. Holden, S. Houck, X. Huang, K. Hui, B. C. Huynh, M. Ivanov, Á. Jász, H. Ji, H. Jiang, B. Kaduk, S. Kähler, K. Khistyayev, J. Kim, G. Kis, P. Klunzinger, Z. Koczor-Benda, J. H. Koh, D. Kosenkov, L. Koulias, T. Kowalczyk, C. M. Krauter, K. Kue, A. Kunitsa, T. Kus, I. Ladjánszki, A. Landau, K. V. Lawler, D. Lefrancois, S. Lehtola, R. R. Li, Y. P. Li, J. Liang, M. Liebenthal, H. H. Lin, Y. S. Lin, F. Liu, K. Y. Liu, M. Loipersberger, A. Luenser, A. Manjanath, P. Manohar, E. Mansoor, S. F. Manzer, S. P. Mao, A. V. Marenich, T. Markovich, S. Mason, S. A. Maurer, P. F. McLaughlin, M. F. S. J. Menger, J. M. Mewes, S. A. Mewes, P. Morgante, J. W. Mullinax, K. J. Oosterbaan, G. Paran, A. C. Paul, S. K. Paul, F. Pavošević, Z. Pei, S. Prager, E. I. Proynov, Á. Rák, E. Ramos-Cordoba, B. Rana, A. E. Rask, A. Rettig, R. M. Richard, F. Rob, E. Rossomme, T. Scheele, M. Scheurer, M. Schneider, N. Sergueev, S. M. Sharada, W. Skomorowski, D. W. Small, C. J. Stein, Y. C. Su, E. J. Sundstrom, Z. Tao, J. Thirman, G. J. Tornai, T. Tsuchimochi, N. M. Tubman, S. P. Veccham, O. Vydrov, J. Wenzel, J. Witte, A. Yamada, K. Yao, S. Yeganeh, S. R. Yost, A. Zech, I. Y. Zhang, X. Zhang, Y. Zhang, D. Zuev, A. Aspuru-Guzik, A. T. Bell, N. A. Besley, K. B. Bravaya, B. R. Brooks, D. Casanova, J. D. Chai, S. Coriani, C. J. Cramer, G. Cserey, A. E. DePrince, R. A. DiStasio, A. Dreuw, B. D. Dunietz, T. R. Furlani, W. A. Goddard, S. Hammes-Schiffer, T. Head-Gordon, W. J. Hehre, C. P. Hsu, T. C. Jagau, Y. Jung, A. Klamt, J. Kong, D. S. Lambrecht, W. Liang, N. J. Mayhall, C. W. McCurdy, J. B. Neaton, C. Ochsenfeld, J. A. Parkhill, R. Peverati, V. A. Rassolov, Y. Shao, L. V. Slipchenko, T. Stauch, R. P. Steele, J. E. Subotnik, A. J. W. Thom, A. Tkatchenko, D. G. Truhlar, T. Van Voorhis, T. A. Wesolowski, K. B. Whaley, H. L. Woodcock, P. M. Zimmerman, S. Faraji, P. M. W. Gill, M. Head-Gordon, J. M. Herbert and A. I. Krylov, *J Chem Phys*, 2021, **155**, 084801.